

# Supplementary Information

## **Unravelling Charge-transfer in Pd to pyrrolic-N bond for superior electrocatalytic performance**

Lipipuspa Sahoo,<sup>1</sup> Sanjit Mondal,<sup>1</sup> A. Gloskovskii,<sup>2</sup> Arunabhiram Chutia,<sup>3,\*</sup> Ujjal K. Gautam<sup>1,\*</sup>

<sup>1</sup>Department of Chemical Sciences, Indian Institute of Science Education and Research (IISER)-Mohali, Sector 81, Mohali, SAS Nagar, Punjab 140306, India

<sup>2</sup>DESY Photon Science, Deutsches Elektronen-Synchrotron, 22603 Hamburg, Germany

<sup>3</sup>School of Chemistry, University of Lincoln, Lincoln LN6 7TS, United Kingdom

\* [ujjalgautam@gmail.com](mailto:ujjalgautam@gmail.com), [ujjalgautam@iisermohali.ac.in](mailto:ujjalgautam@iisermohali.ac.in), [achutia@lincoln.ac.uk](mailto:achutia@lincoln.ac.uk), [achutia@gmail.com](mailto:achutia@gmail.com)

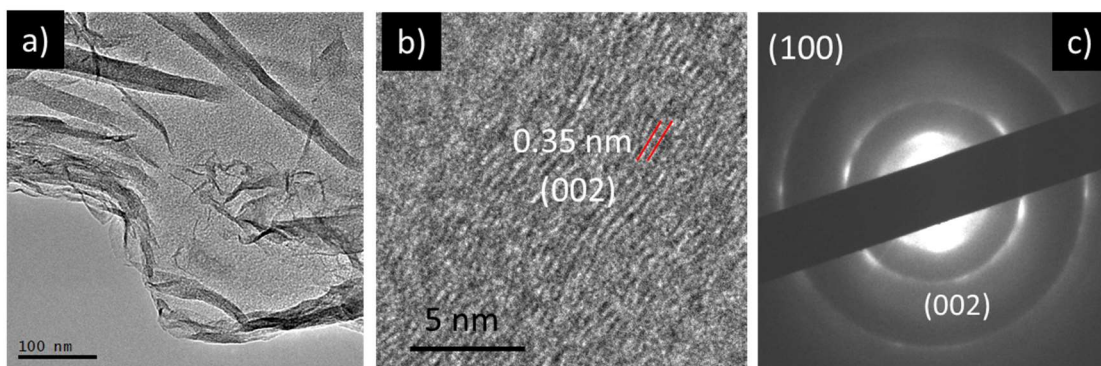


**Fig. S1** Microscopic characterization of NRGO: a) TEM image, b) high-resolution TEM image depicting (002) planes, c) selected area electron diffraction pattern showing (002) and (100) planes.

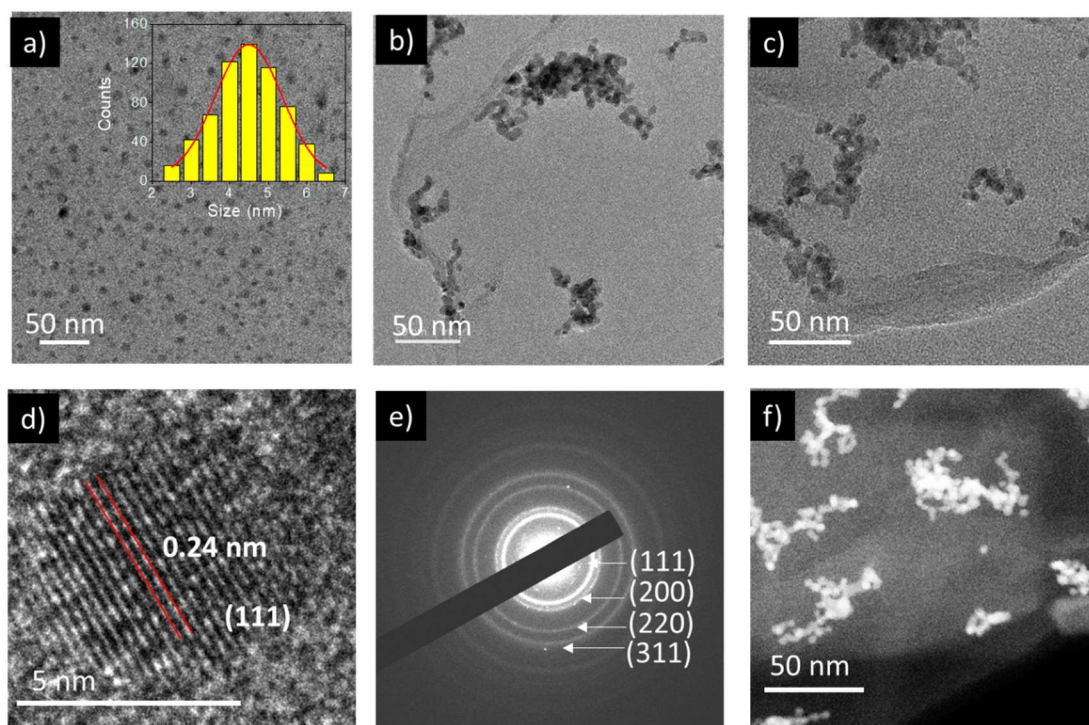


**Fig. S2** (a) TEM image of bare Pd NCs. Inset shows the particle size distribution. Pd/NRGO *ex-situ* (32% Pd loading) sample: (b,c) low magnification TEM images highlighting the clusters of Pd NCs, (d) high-resolution TEM image of a particle showing the (111) planes of Pd, (e) SAED pattern, (f) HAADF-STEM image for the same sample.

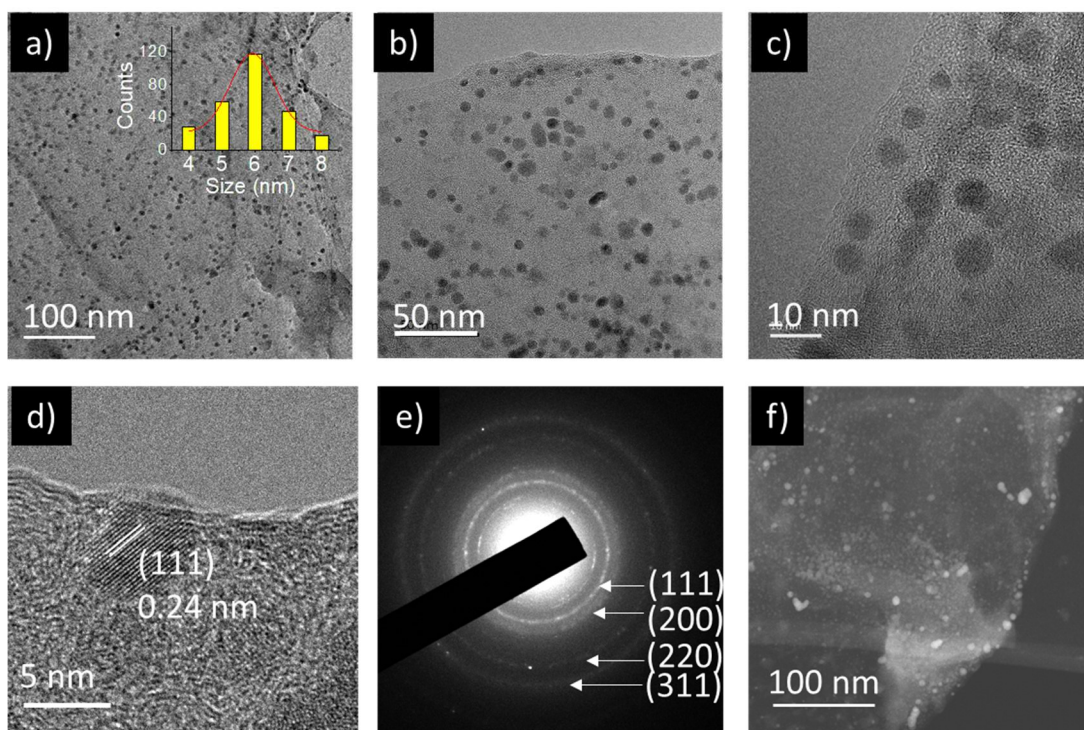


**Fig. S3** Microscopic characterization of Pd/RGO (*in-situ*, 32% Pd loading): (a,b,c) low magnification TEM images. Inset in (a) shows the particle size distribution. (d) HRTEM image of a particle showing the (111) planes of Pd, (e) SAED pattern acquired on the Pd NCs. (f) HAADF-STEM image of the composite. .

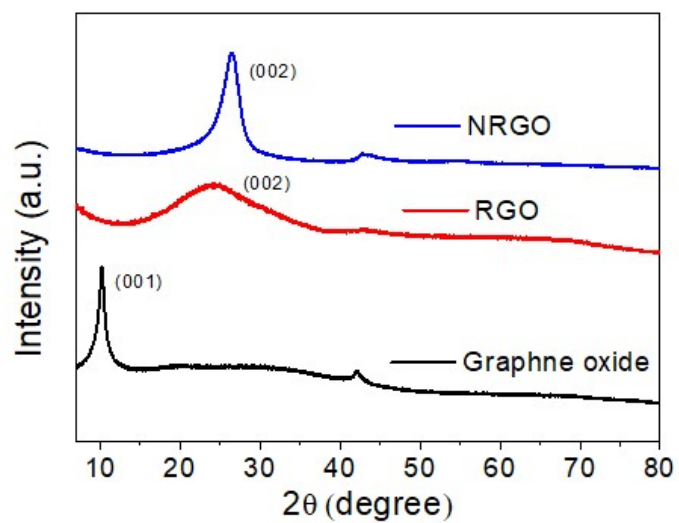


**Fig. S4.** PXRD patterns of graphene oxide, RGO and NRGO.

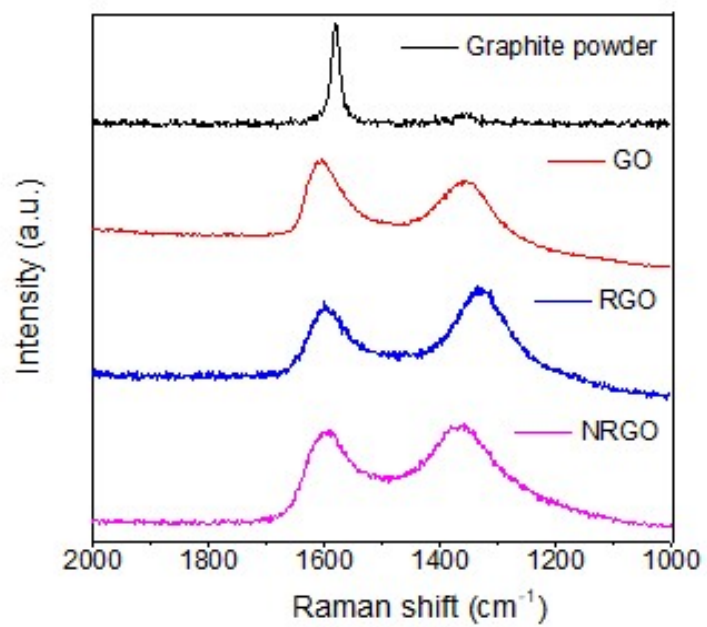


**Fig. S5** Raman spectra of graphite powder, graphene oxide, RGO and NRGO.

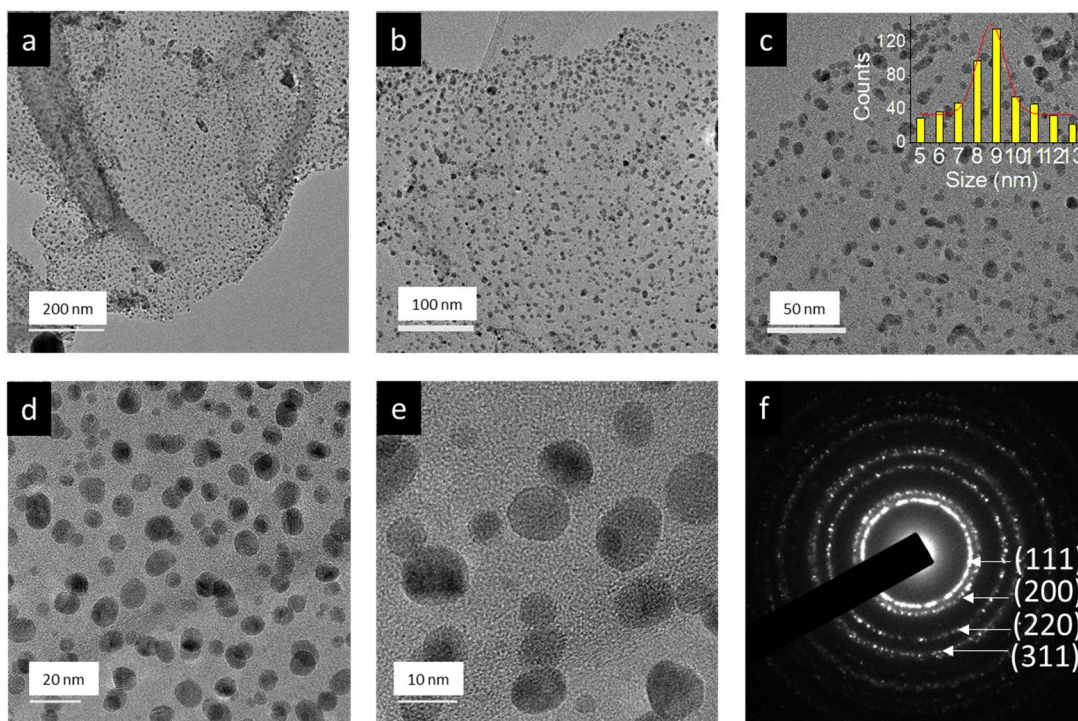


**Fig. S6** Microscopic characterization of Pd/NRGO *in-situ* (22% Pd loading): (a,b,c) low magnification TEM images. Inset in (c) depicts the particle size distribution. (d,e) high magnification TEM images, (f) the corresponding SAED pattern.

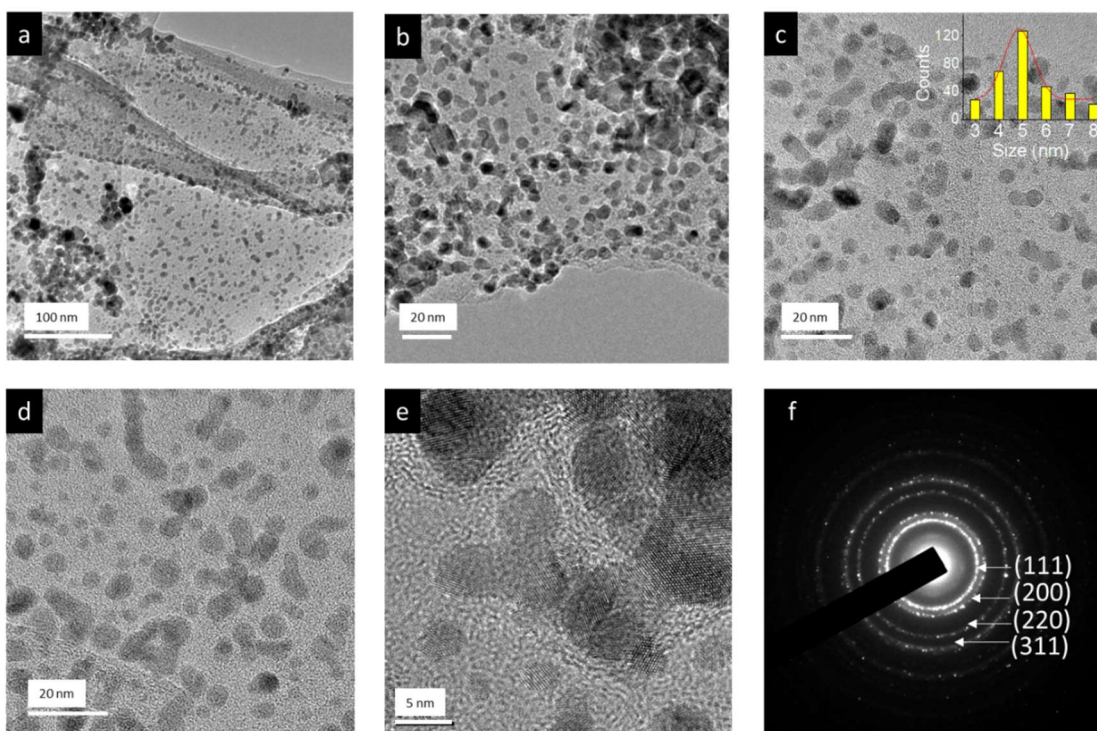


**Fig. S7** Microscopic characterization of Pd/NRGO (*in-situ*, 47% Pd loading): (a-d) low magnification TEM images. Inset in c depicts the Pd particle size distribution. (e) high magnification TEM image and (f) the corresponding SAED pattern.

**Supplementary Note-1:** The kinetic currents of the different catalysts were first calculated from the ORR polarization curves by following the Koutecky–Levich (K-L) equation and then divided with Pt/Pd mass and ECSA to obtain the mass and specific activities ( $I_{k,\text{mass}}$  and  $I_{k,\text{specific}}$ ), respectively (see experimental section). Fig. S8a shows the LSV plots for the Pd/NRGO *in-situ* sample (32% loading) recorded by using different electrode rotation rates (per minute or rpm) in  $\text{O}_2$  saturated 0.1 M KOH and the corresponding K-L plot is given in Fig. S8b. The comparable slopes at the various applied potentials (0.75-0.9 V range vs. RHE) imply that the ORR kinetics follows a first-order kinetics. The corresponding electron transfer number ( $n$ ) was found to be  $\sim 4.0$  confirming a complete reduction of  $\text{O}_2$  to water on the Pd/NRGO surface. Similarly,  $n$  was calculated to be  $\sim 4$  for other materials also from the respective K-L plots (Fig. S9-13)

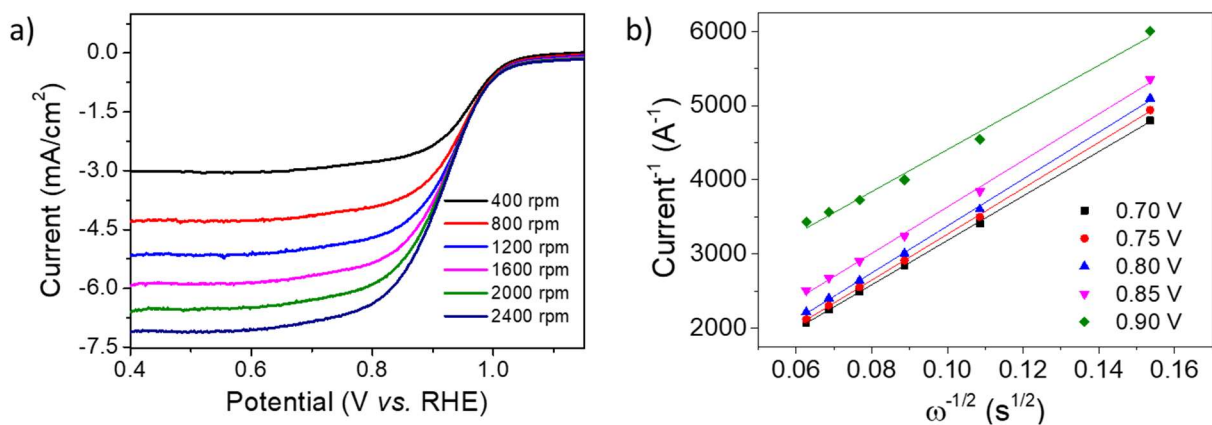


**Fig. S8** a) ORR polarization curves of Pd/NRGO *in-situ* sample (32% loading) at different rotation rates in O<sub>2</sub> saturated 0.1 M KOH with a scan-rate of 10 mV/s, b) the corresponding K-L plots at different potentials w.r.t. RHE.

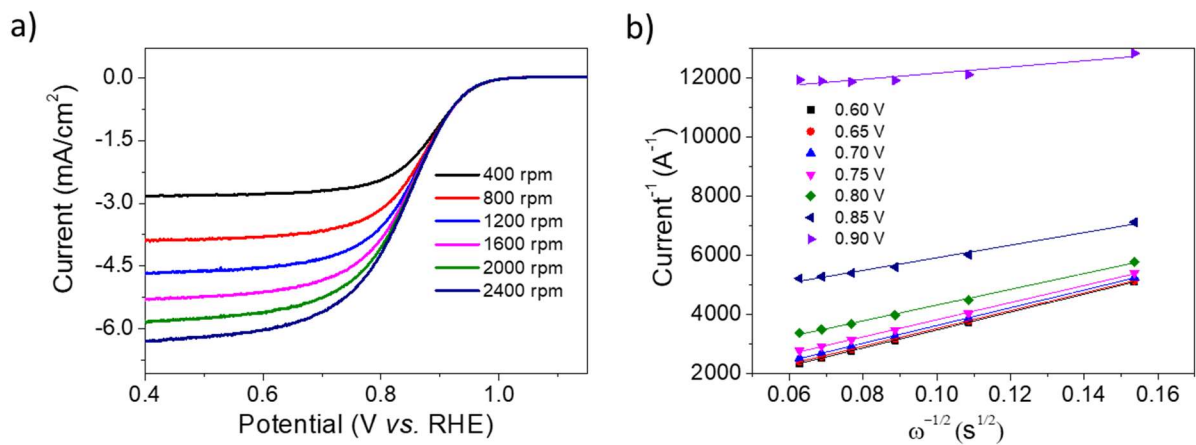


**Fig. S9** a) ORR polarization curves of Pd/NRGO *in-situ* sample (22% loading) at different rotation rates in O<sub>2</sub> saturated 0.1 M KOH with a scan-rate of 10 mV/s, b) the corresponding K-L plots at different potentials w.r.t. RHE.

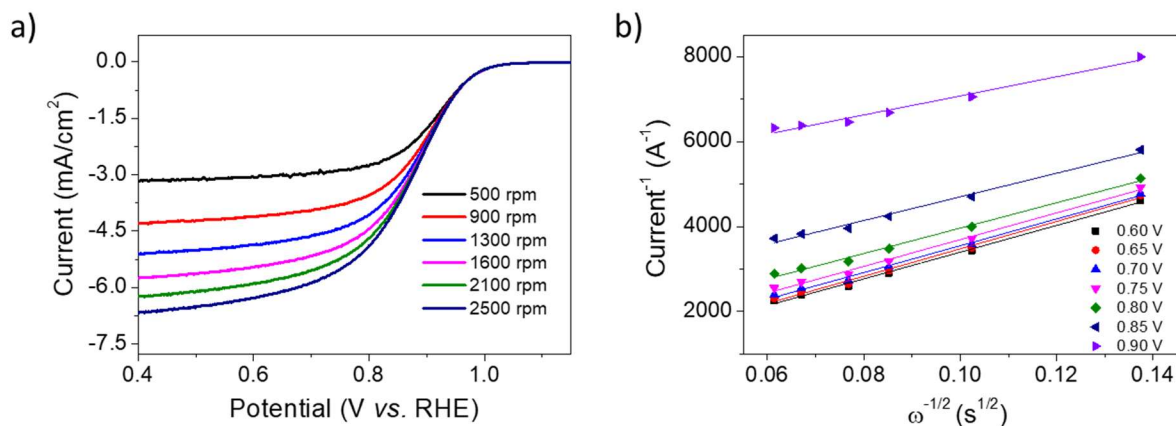


**Fig. S10** a) ORR polarization curves of Pd/NRGO *in-situ* sample (47% loading) at different rotation rates in O<sub>2</sub> saturated 0.1 M KOH with a scan-rate of 10 mV/s, b) the corresponding K-L plots at different potentials w.r.t. RHE.

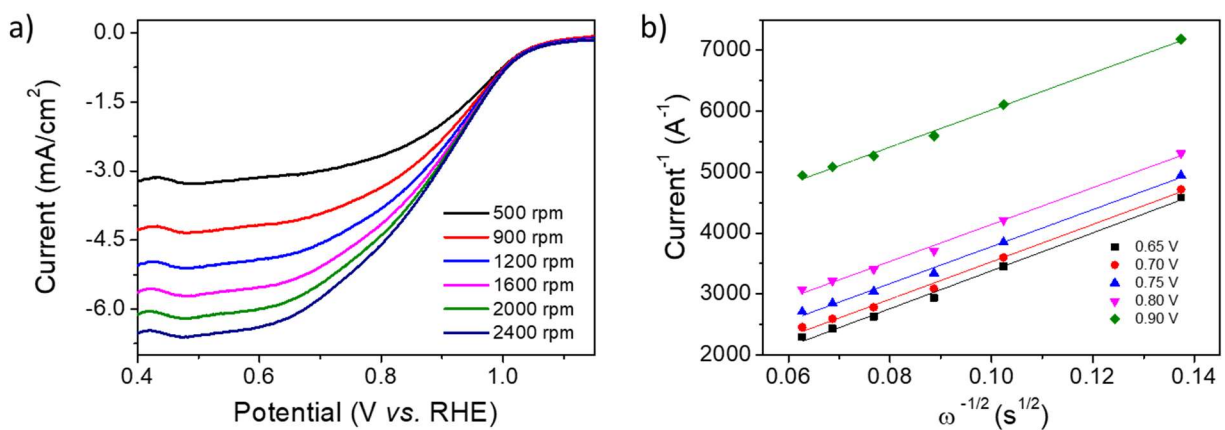


**Fig. S11** a) ORR polarization curves of Pd/NRGO *ex-situ* (32% loading) sample at different rotation rates in O<sub>2</sub> saturated 0.1 M KOH with a scan rate of 10 mV/s, b) the corresponding K-L plots at different potentials w.r.t. RHE.

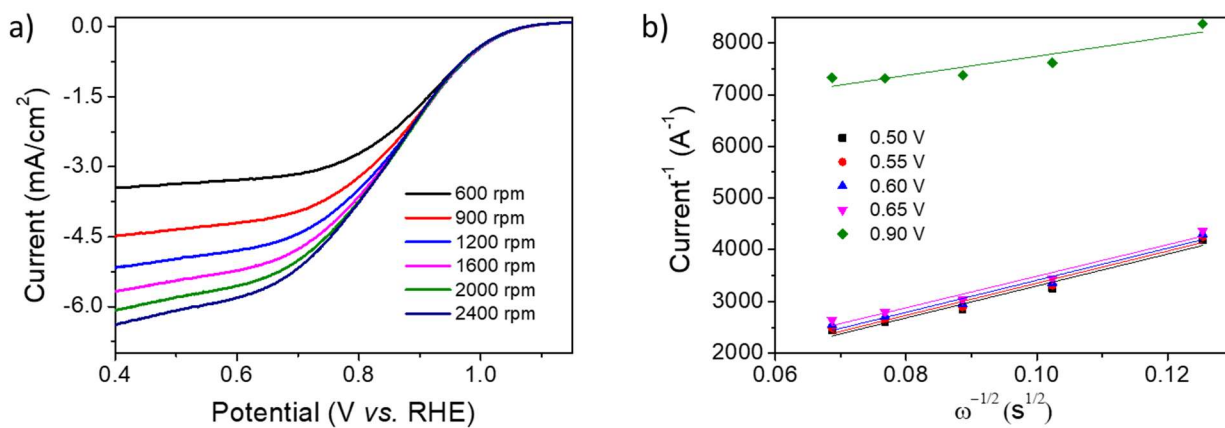


**Fig. S12** a) ORR polarization curves of Pd/RGO (*in-situ*) at different rotation rates in O<sub>2</sub> saturated 0.1 M KOH with a scan rate of 10 mV/s, b) the corresponding K-L plot at different potential w.r.t. RHE.

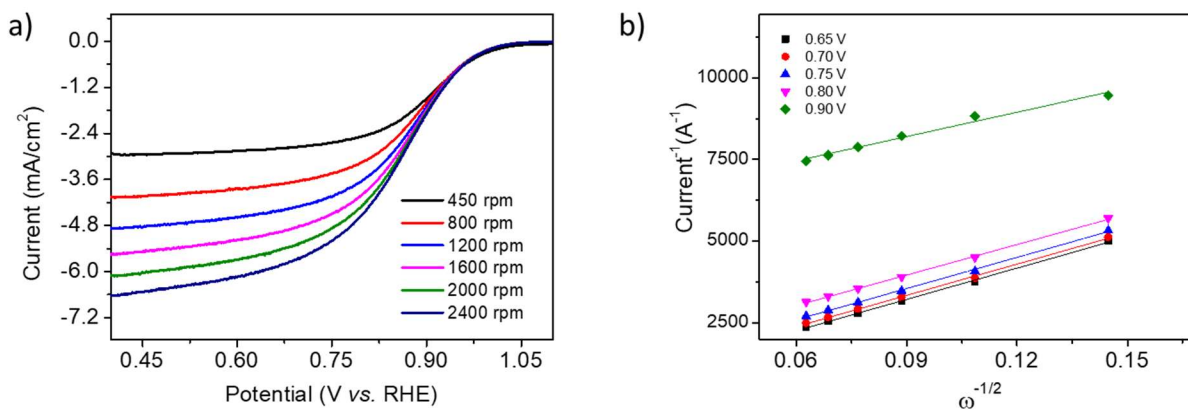


**Fig. S13** a) ORR polarization curve of Pt/C at different rotation rates in O<sub>2</sub> saturated 0.1 M KOH with a scan rate of 10 mV/s, b) the corresponding K-L plots at different potentials w.r.t. RHE.

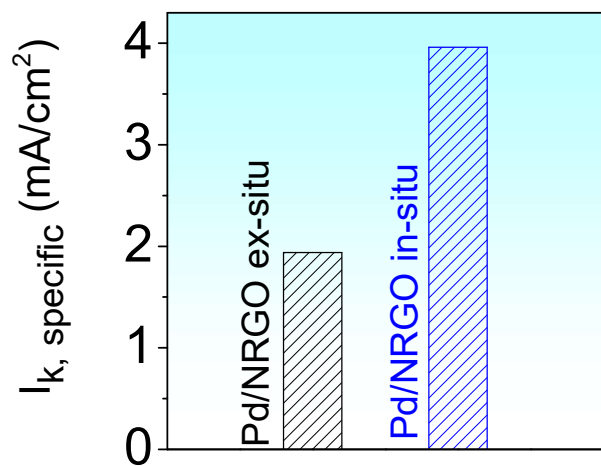


**Fig. S14** Specific activities of Pd/NRGO in-situ, Pd/NGO ex-situ and commercial Pt/C at 0.9 V vs. RHE.

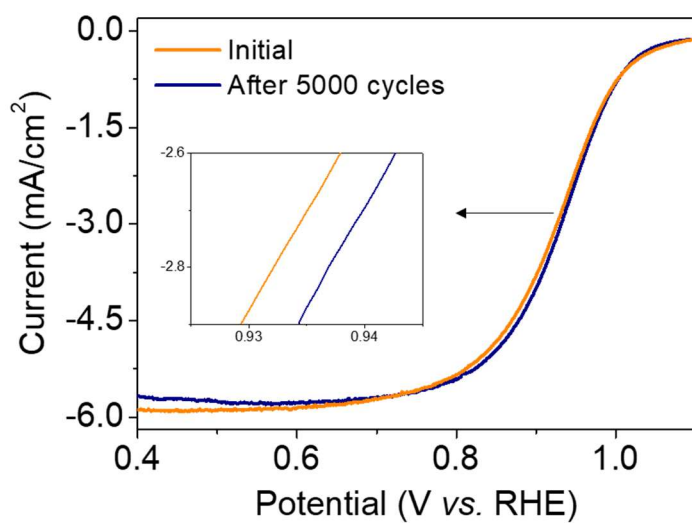


**Fig. S15** ORR polarization curves of Pd/NRGO *in-situ* sample (32% loading) before and after 5000 CV cycles.

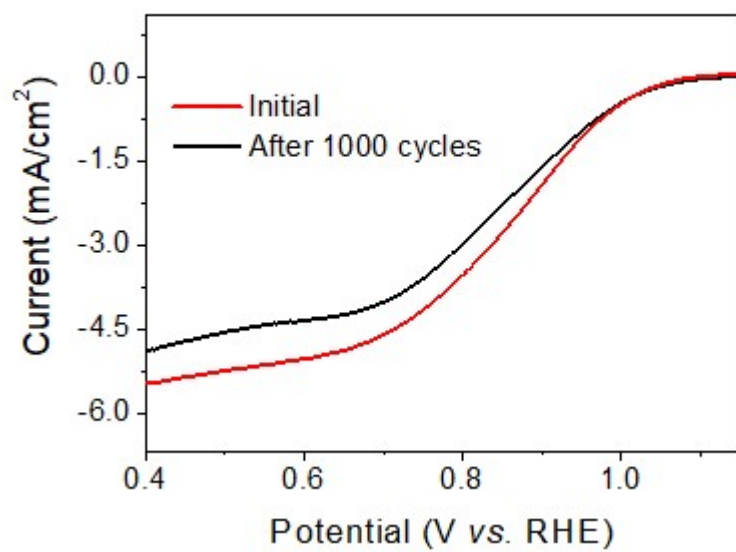


**Fig. S16** ORR polarization curves of Pd/RGO (*in-situ*) before and after 1000 CV cycles.

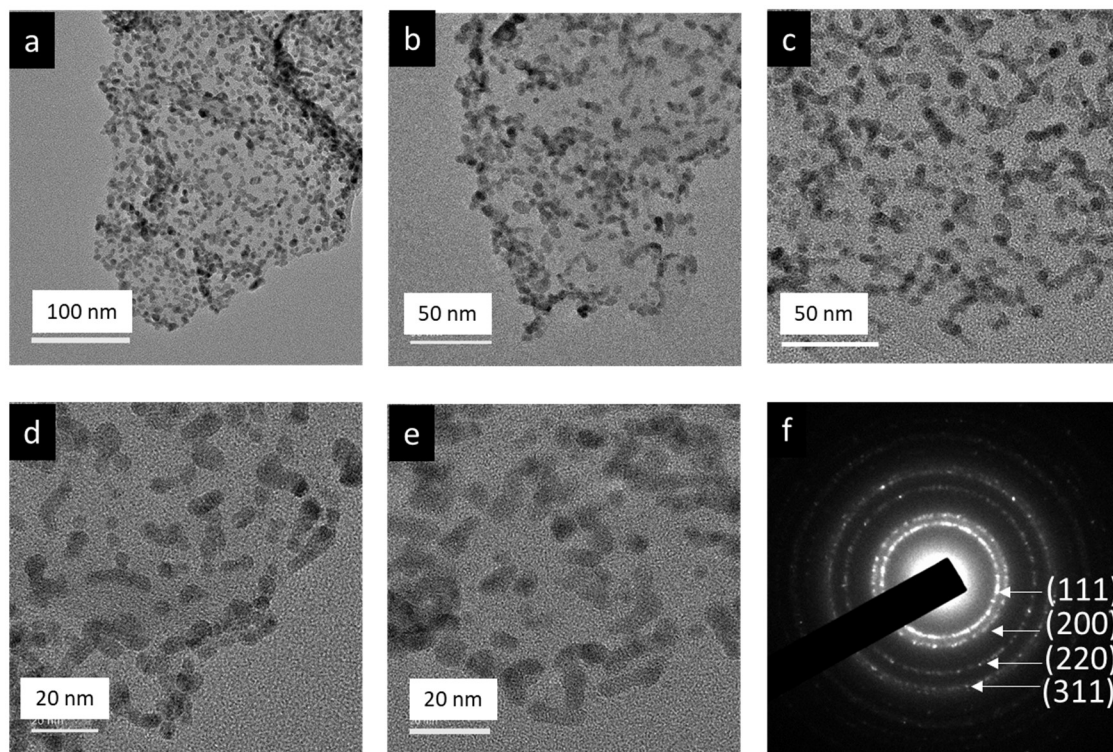


**Fig. S17** Low magnification TEM images (a-d), high magnification TEM images (d,e) and SAED pattern (f) of Pd/NRGO *in-situ* sample (32% loading) after 15000 CV cycles.

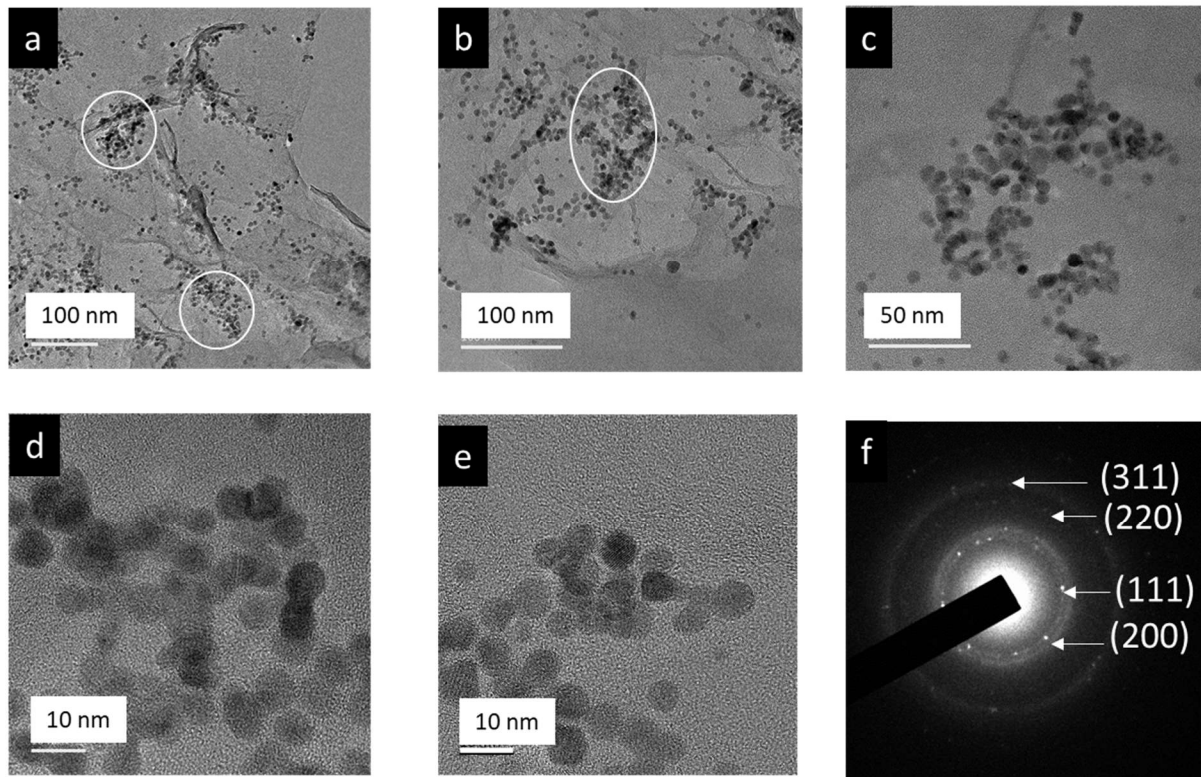


**Fig. S18** TEM images of Pd/RGO (*in-situ*) at different magnifications after use in 1000 ORR CV cycles (a-e) and the corresponding SAED pattern (f). Circles in (a,b) are typical Pd NC clusters seen throughout the sample. Such clusters were rarely found in the Pd/NRGO *in-situ* sample after 15000 CV cycles.

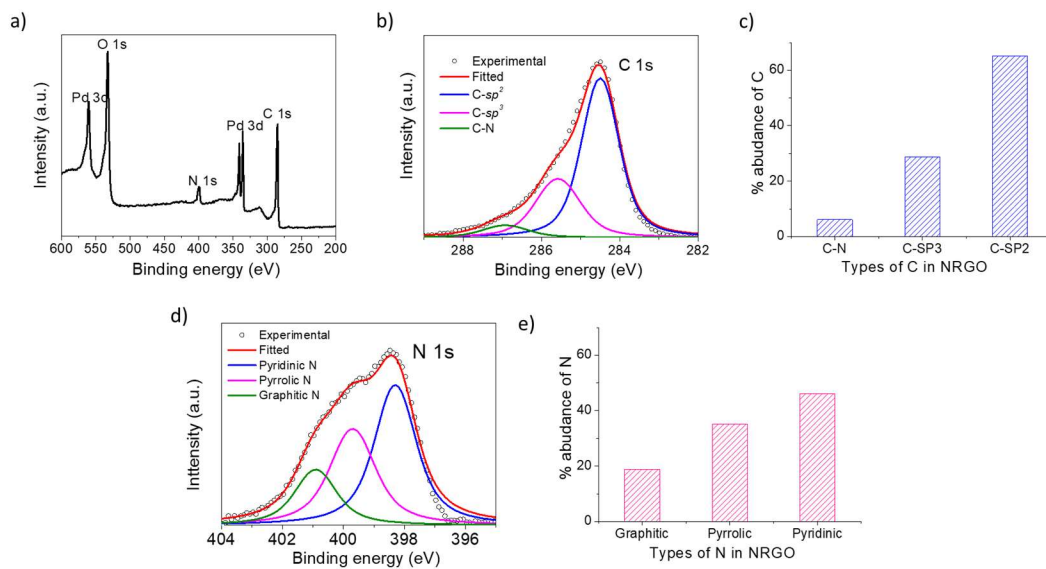


**Fig. S19** XPS analysis of the Pd/NRGO *in-situ* sample (32% loading): a) the survey spectrum; the HR-HAXPES spectra of b) C 1s, c) percentage of abundance of the different C, d) High resolution HAXPES spectrum of N 1s of Pd/NRGO *in-situ* sample and e) percentage of abundance of the different N species in the sample.

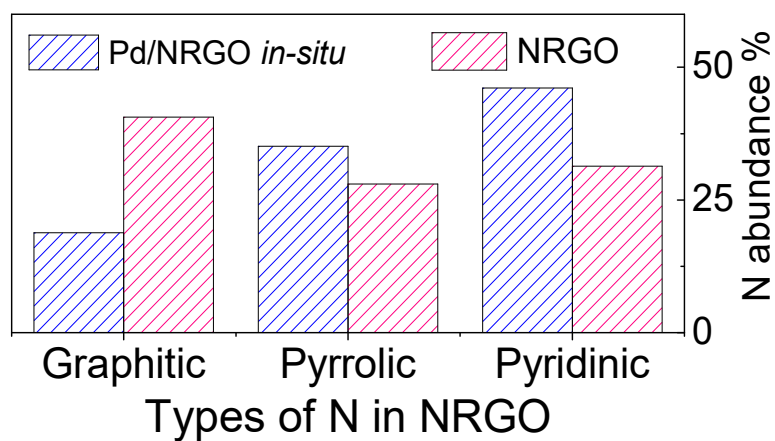


**Fig. S20** Relative abundance of different N moieties in NRGO and Pd/NRGO *in-situ* sample.

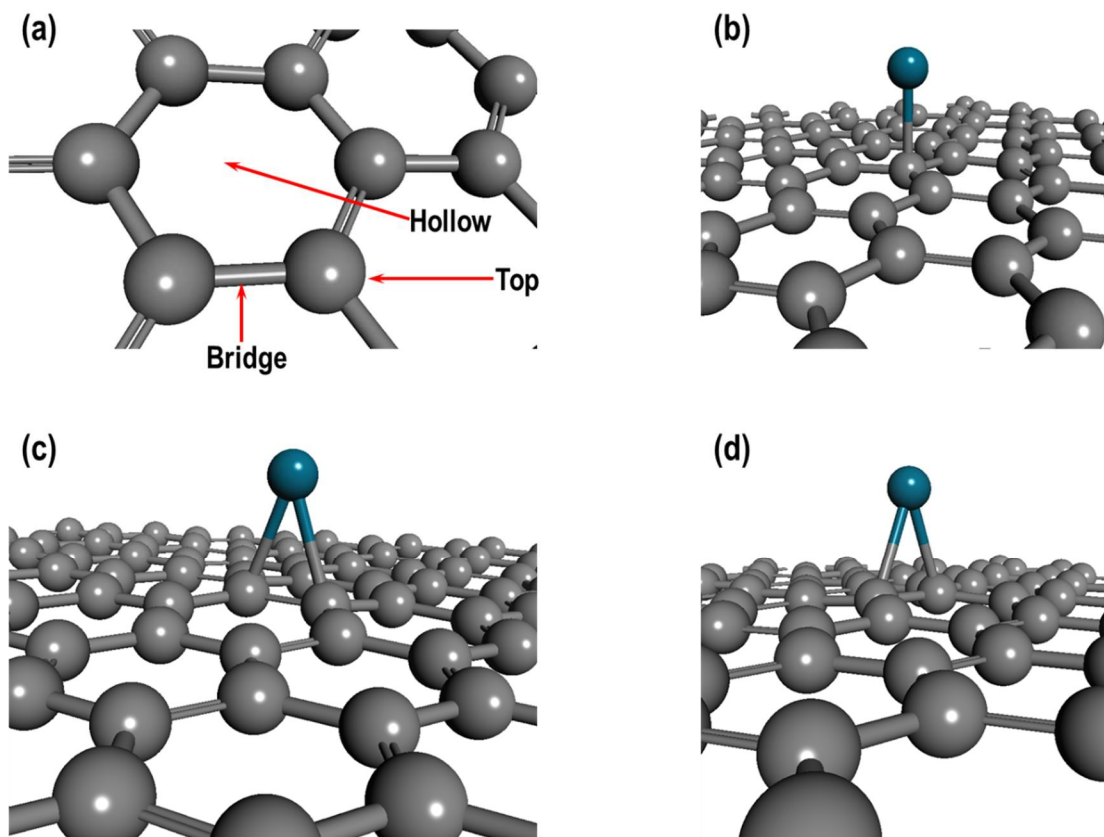


**Fig. S21** (a) Adsorption sites of Pd on graphene (G). Fully optimised structures of Pd (b) on top, (b) bridge and (c) hollow sites of pristine graphene. For clarity the active sites have been zoomed-in and the periodic boundaries have been omitted.

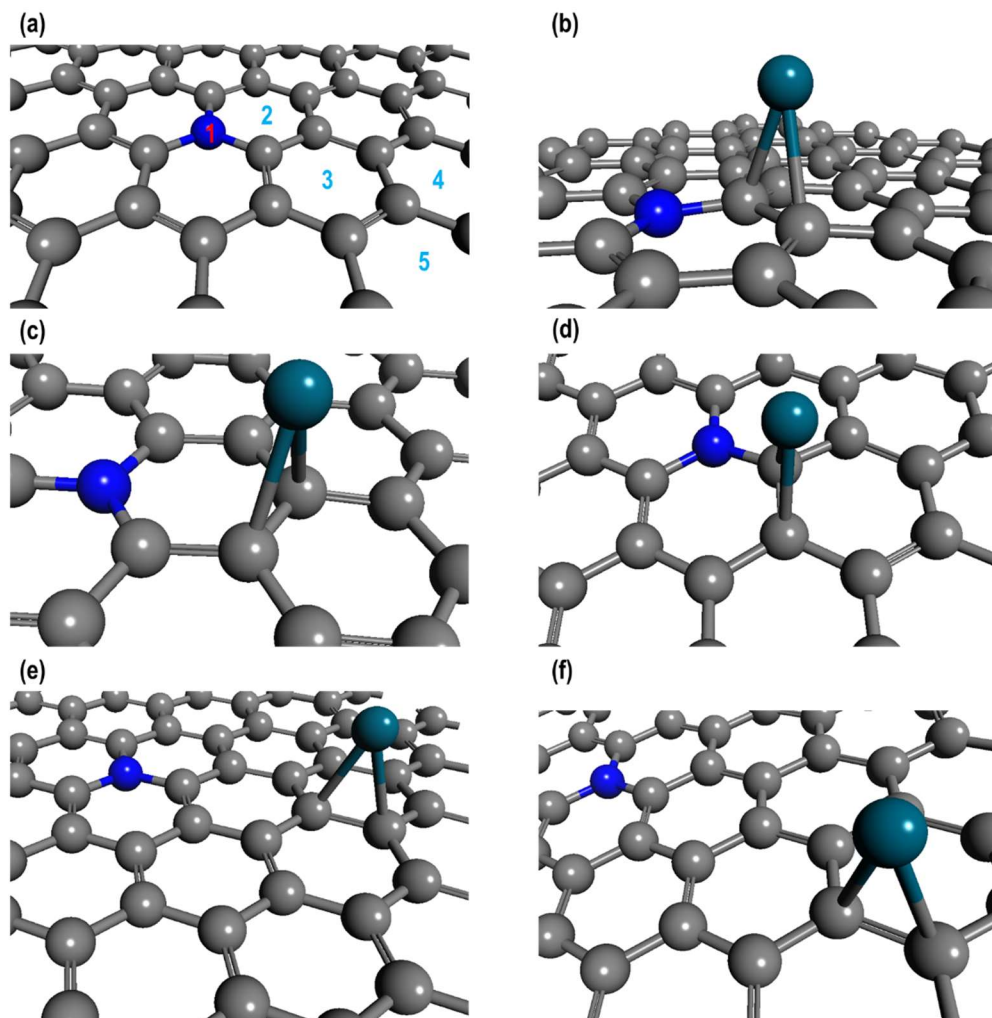


**Fig. S22** (a) Adsorption sites of Pd on NG. Fully optimised structures of (b) Conf-1, (c) Conf-2, (d) Conf-3, (e) Conf-4, (f) Conf-5. For clarity the active sites have been zoomed-in and the periodic boundaries have been omitted.

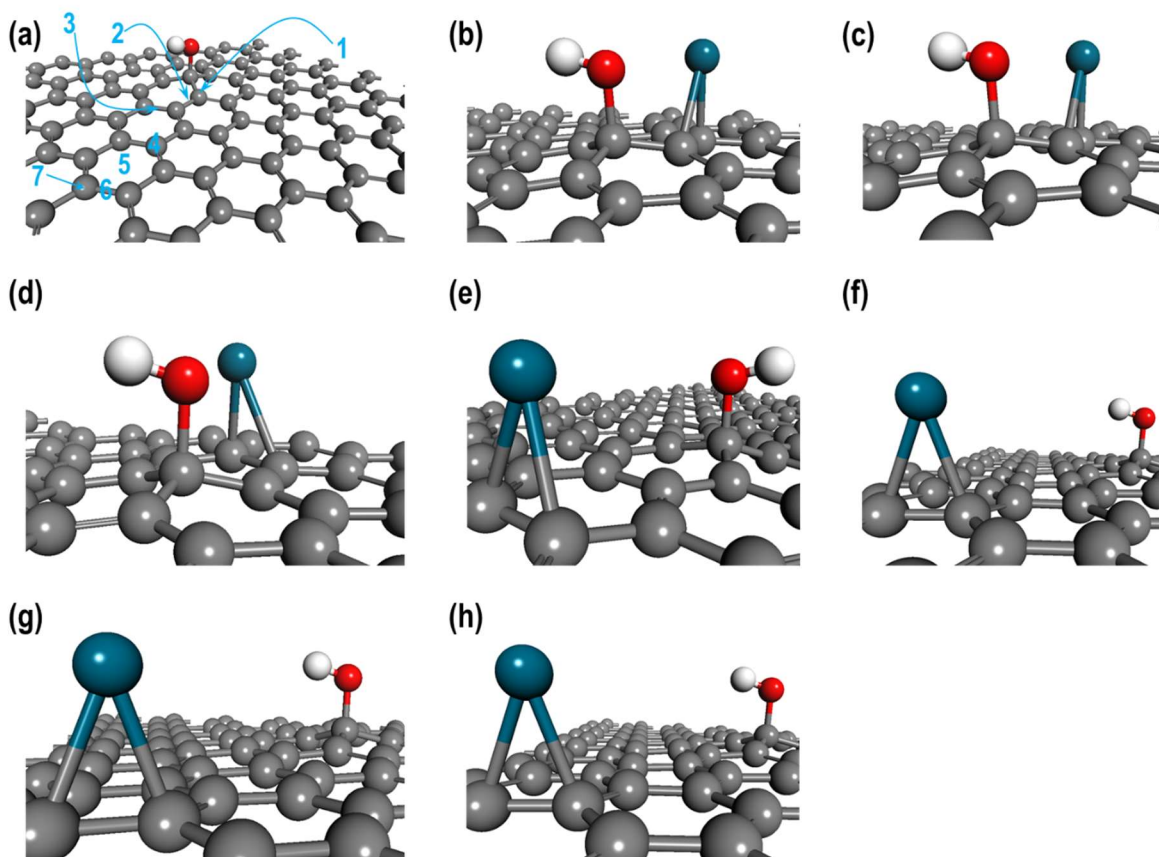


**Fig. S23** (a) Adsorption sites of Pd on  $G_{OH}$ . Fully optimised structures of (b) Conf-1, (c) Conf-2, (d) Conf-3, (e) Conf-4, (f) Conf-5, (g) Conf-6, and (h) Conf-7. For clarity the active sites have been zoomed-in and the periodic boundaries have been omitted.

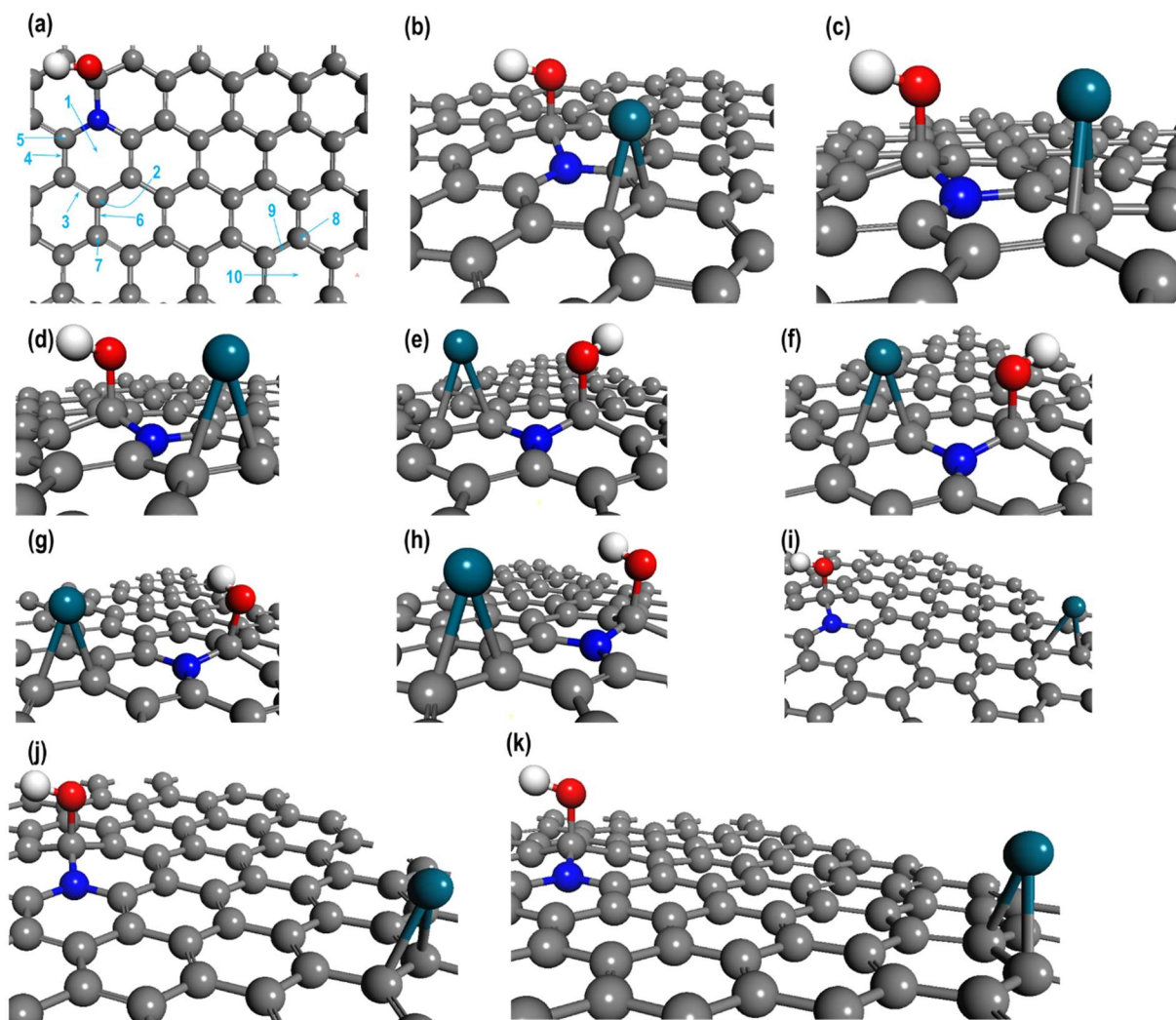


**Fig. S24** Top view of (a) various adsorption sites of Pd adatom on the  $N_G-OH$ . Fully relaxed structures of Pd adatom on (b) Conf-1, (c) Conf-2, (d) Conf-3, (e) Conf-4, (f) Conf-5, (g) Conf-6, (h) Conf-7, (i) Conf-8, (k) Conf-9, and (k) Conf-10. For clarity the active sites have been zoomed-in and the periodic boundaries have been omitted.

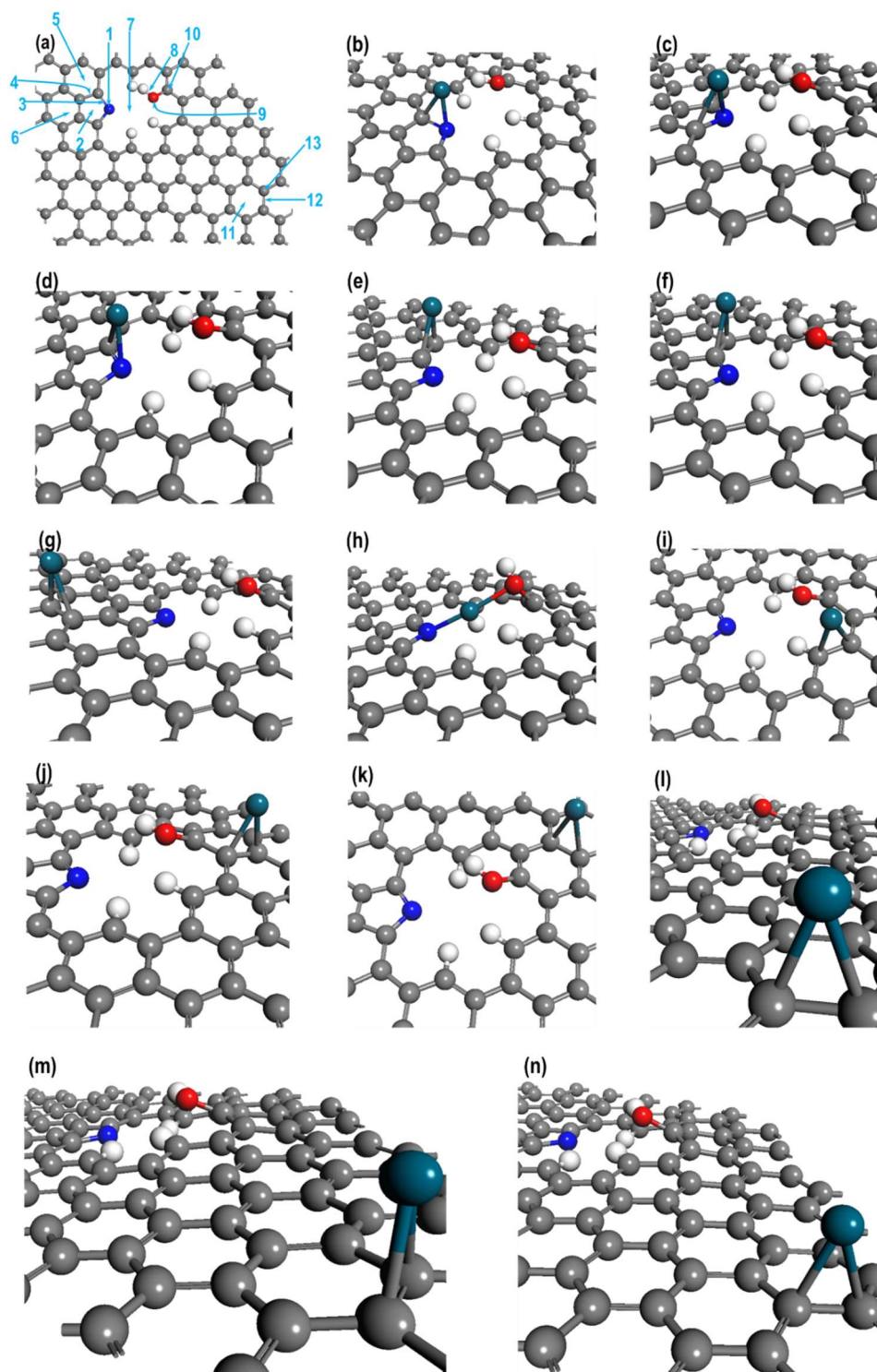


**Fig. S25** Top view of (a) various adsorption sites of Pd adatom on the  $N_{\text{Pyr-OH}}$ . Fully relaxed structures of Pd adatom on (b) Conf-1, (c) Conf-2, (d) Conf-3, (e) Conf-4, (f) Conf-5, (g) Conf-6, (h) Conf-7, (i) Conf-8, (j) Conf-9, (k) Conf-10, (l) Conf-11, (m) Conf-12 and (n) Conf-13. For clarity the active sites have been zoomed-in and the periodic boundaries have been omitted.

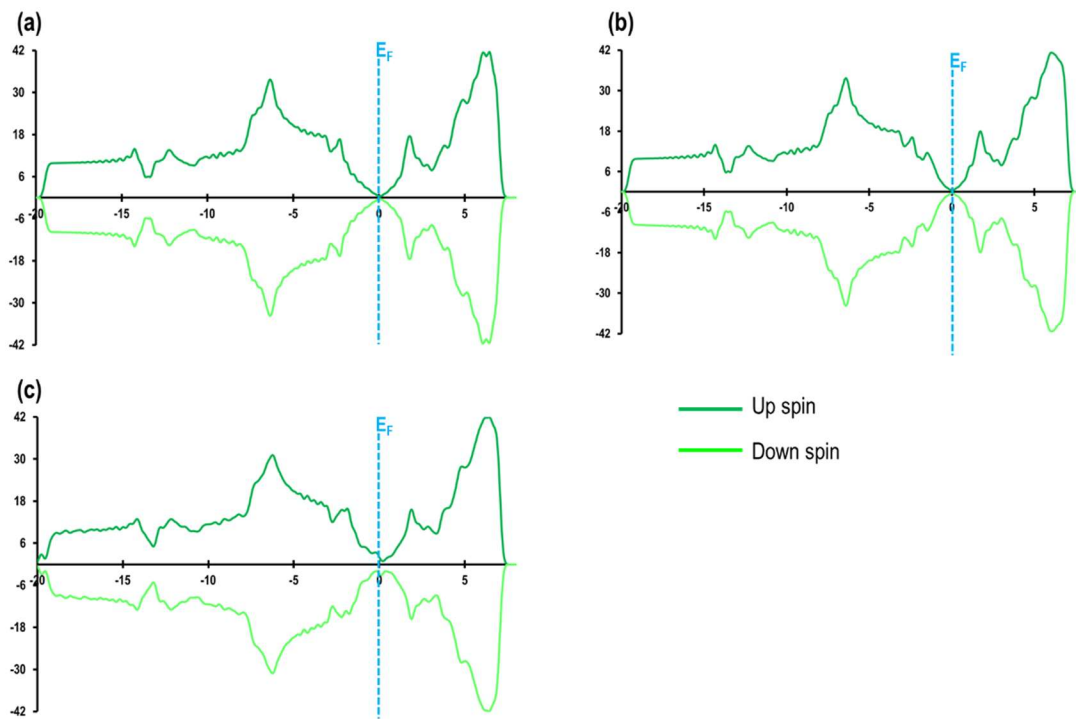


**Fig. S26.** The total density of states for (a) pristine graphene, (b) Pd/ G and (c) Pd/  $N_{PyT-OH}$ .

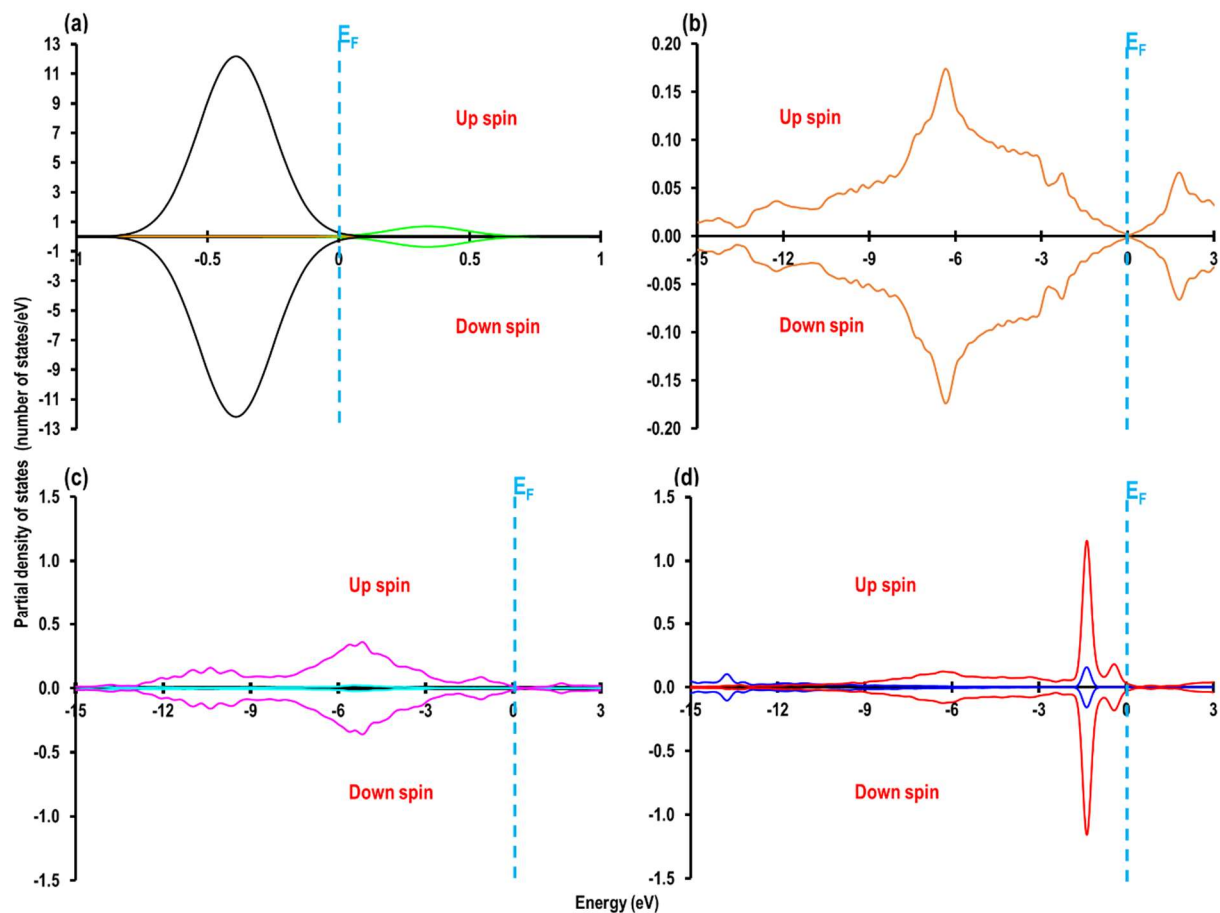


**Fig. S27** The partial density of states of (a) Pd  $d$  and  $s$ -orbital signatures of Pd atom, (b) C  $p$ -orbital signatures of G, (c) N  $p$ -orbital of pyrrole ring and (d) O  $p$ -orbital of OH group of  $N_{\text{Pyr-OH}}$ . The Fermi energy ( $E_F$ ) is indicated by a dotted line at 0 eV.

**Supporting Note 2.** The models used to check the five preferable positions (a) P1, (b) P2, (c) P3, (d) P4, and (e) P5 of the  $-OH$  group on the  $N_G$ . For clarity the active sites have been zoomed-in and the periodic boundaries have been omitted.

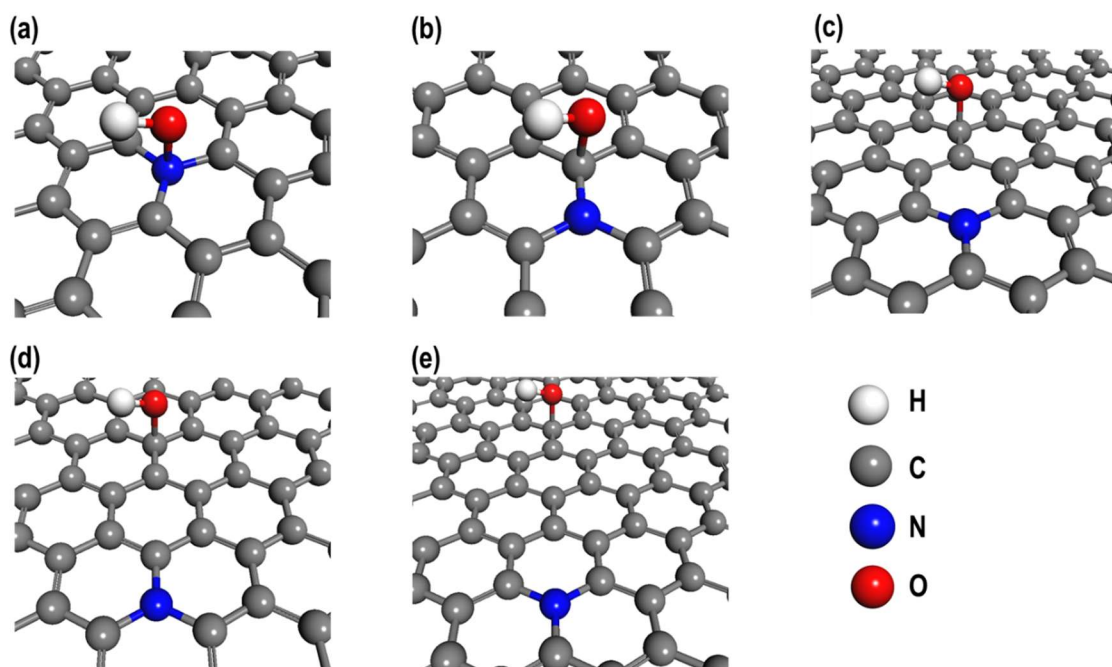


**Table S1.** Comparison of ORR performance of Pd/NRGO in-situ with recently reported literature data.

Sl. No.	Materials	$E_{1/2}$ (V vs RHE)	Electrolyte	Mass activity	Stability	Reference
<b>1</b>	<b>Pd/NRGO</b>	<b>0.935</b>	<b>0.1 M KOH</b>	<b>0.59 A/mg</b>	<b>28% decrease in mass activity 15000 cycle (33 h)</b>	<b>This work</b>
2	Pd <sub>72</sub> Cu <sub>28</sub> mesoporous nanospheres	0.89	0.1 M KOH	0.19 A/mg @0.85 V	4% mass activity decrease after 3000 cycle	ACS Appl. Mater. Interfaces 2019, 11, 36544–36552
3	Pd-Ru@NG	0.8	0.1 M KOH	-	Current retained 80% after 2000 sec	<i>Chem. Commun.</i> , 2019, 55, 13928--13931
4	Pd <sub>59</sub> Cu <sub>30</sub> Co <sub>11</sub>	0.91	0.1 M KOH	0.38 A/mg	32% decrease in mass activity after 15000 cycles	Nat. Commun. 2018, 9, 3702.
5	PdBi	0.92	0.1 M KOH	0.95 A/mg	40% mass activity decrease after 10000 cycle	ACS Energy Lett. 2020, 5, 17–22
6	Ni@Pd <sub>3</sub> NCs	0.86	0.1 M KOH	0.035 A/mg	5% mass activity decrease after 3000 cycles	J. Mater. Chem. A, 2017, 5, 9233-9240
7	Pd-Co nanocrystals on N doped porous C	0.845	0.1 M KOH	0.45 A/mg	8% current decrease after 20000 s,	J. Mater. Chem. A, 2017, 5, 10876–10884
8	Ordered PdCuCo/C Nanoparticle	0.872	0.1 M NaOH	0.13 A/mg	5% mass activity decrease after 10000 cycles	Angew. Chem. Int. Ed. 55, 9030-9035 (2016)
9	Pd nanocluster on carbon sheet	0.8	0.1 M KOH		4mV $E_{1/2}$ decrease after 5000 cycles	<i>ChemElectroChem</i> 2 017, 4, 1349.
10	Pd NCs on N-doped graphene quantum dot	0.8	0.1 M KOH		-	<i>ACS Sustainable Chem. Eng.</i> 2016, 4, 6580
11	PdNiCu/NG	0.8	0.1 M KOH		30 mV $E_{1/2}$ decrease after 5000 cycles	<i>Electrochimica Acta</i> 235 (2017) 543–552

**Table S2.** Calculated adsorption energies of Pd adatom adsorption on G, N<sub>G</sub>, G<sub>OH</sub>, N<sub>G-OH</sub>, N<sub>pyr-OH</sub>.

System	E <sub>ad</sub> (eV)
Pd on G	
Conf-1	-1.640
<b>Conf-2</b>	<b>-1.699</b>
Conf-3	-1.698
Pd on N <sub>G</sub>	
Conf-1	-1.697
<b>Conf-2</b>	<b>-1.709</b>
Conf-3	-1.698
Conf-4	-1.681
Conf-5	-1.690
Pd on G <sub>OH</sub>	
Conf-1	-1.964
Conf-2	-1.965
<b>Conf-3</b>	<b>-2.039</b>
Conf-4	-1.738
Conf-5	-1.716
Conf-6	-1.717
Conf-7	-1.717
Pd on N <sub>G-OH</sub>	
Conf-1	-1.745
Conf-2	-1.744
Conf-3	-1.737
<b>Conf-4</b>	<b>-1.750</b>
Conf-5	-1.749
Conf-6	-1.740
Conf-7	-1.738
Conf-8	-1.715
Conf-9	-1.704
Conf-10	-1.719
Pd on N <sub>pyr-OH</sub>	
Conf-1	-2.011
Conf-2	-1.966
Conf-3	-2.011
Conf-4	-2.075
Conf-5	-2.076
Conf-6	-1.673
<b>Conf-7</b>	<b>-2.516</b>
Conf-8	-1.996
Conf-9	-1.832

Conf-10	-1.628
Conf-11	-1.732
Conf-12	-1.732
Conf-13	-1.737

---

**Table S3.** Summary of the adsorption energy for the most stable configurations of Pd on G, N<sub>G</sub>, G<sub>OH</sub>, N<sub>G-OH</sub>, N<sub>pyr-OH</sub>.

<b>System</b>	<b>E<sub>ad</sub> (eV)</b>
Pd on G	-1.699
Pd on N <sub>G</sub>	-1.709
Pd on G <sub>OH</sub>	-2.039
Pd on N <sub>G-OH</sub>	-1.750
Pd on N <sub>pyr-OH</sub>	-2.516

**Table S4.** Relative energies of models P1 – P5. Based on the calculated adsorption energy it is concluded that grafting of the OH group is stable next to the N-doped site.

Position of N w.r.t -OH group	Rel. Energy
P1	0.000
P2	-0.027
P3	0.771
P4	0.763
P5	0.886